Fourth International Conference on FRP Composites in Civil Engineering (CICE2008)
22-24July 2008, Zurich, Switzerland

Comparison of measured and calculated interfacial strains at CFRP plate end

A. Schumacher, E. Hack
Swiss Federal Laboratories for Materials Testing and Research (Empa), Dübendorf, Switzerland

ABSTRACT: Small-scale steel beams reinforced with adhesively bonded carbon fiber reinforced polymer (CFRP) plates were subjected to four-point bending. Phase-stepping 3D-digital speckle pattern interferometry (DSPI) was employed to measure the strain concentrations near the end of the CFRP plate, with a special focus on shear and normal strains. Furthermore, a refined finite element analyses (FEA) of the strengthened beam was carried out to predict these strains. Comparisons between measured and calculated strains have confirmed the strong variation of shear strain across the adhesive layer. The FEA has also shown the much higher normal strains present at the adhesive-steel (AS) interface than at the plate-adhesive (PA) interface. This difference has been suggested as the reason why debonding failure more commonly occurs at the AS interface rather than the PA interface.

1 INTRODUCTION

Beams strengthened flexurally with adhesively bonded carbon fiber reinforced polymer (CFRP) plates are susceptible to various failure modes. One of these is the debonding of the plate from the beam, initiated at the plate end. Debonding is caused by high shear and normal interfacial stresses (strains) derived from the transfer of plate tensile forces to the beam. Substantial work has been carried out to model analytically the stress concentrations at the plate end (e.g. Smith & Teng 2001, Rabinovich & Frostig 2000), and, to verify these models, finite element analysis (FEA) tests have also been performed (Teng et al. 2002). Little experimental data is available, however, to verify these analytical and numerical results. This is mainly due to the scant amount of information that is obtained using standard measuring techniques, e.g. electrical resistance strain gauges, where a limited number of discrete measurement points are distributed along the length of the beam. For this reason, an experimental full-field method was applied in the project described herein to produce a more complete comparison between measured and calculated results in the area of interest, that is, the first few millimeters from the plate end.

Non-contact optical methods are increasingly being used as verification for FEA results in mechanical, optical and civil engineering. Both moiré interferometry and speckle methods have been used, e.g. to detect crack initiation from strain profiles in fiber-reinforced composites, to assess strain in composite lap-joints or to measure the strain concentration close to the weld toe of a tubular steel joint. Digital speckle pattern interferometry (DSPI) is well suited for strain analysis due to its high sensitivity, although it can suffer from speckle decorrelation due to rigid body motion, especially for small areas of interest. To overcome this problem, an evaluation method that regains the speckle correlation by image shifting was used to measure the displacement fields (Hack & Schumacher 2007).

For the first time, a comparison of optically measured values to the values of shear and normal strain at the plate end obtained using a FE analysis will be made. Validated knowledge of the shear and normal strains at plate end will aid in the refinement of the existing analytical solutions, which will, in turn, lead to more accurate debonding strength formulations, (e.g. Roberts 1989, Saadatmanesh & Malek 1998) and, consequently, design rules.

2 OPTICAL MEASUREMENTS ON SMALL-SCALE REINFORCED BEAMS

Two 1.0 m long I-section steel beams were strengthened in flexure using two adjacently placed CFRP plates (Fig. 1). Steel beams were used instead of the more commonly tested CFRP strengthened concrete beam in order to preclude cracking, and since steel, with its smoother surface, more often results in better optical measurement results. The properties of the CFRP plates, adhesive and steel beam are given in Table 1. The two steel beams were identical except for the plate and adhesive thicknesses. The beams were loaded with manually controlled hydraulic jacks in a four-point bending arrangement installed on a vibration isolated optical table (Fig. 2 (left)). The loads were distributed to the beams through two 120 mm long steel plates; the beams were supported by 90 mm long plates. For control purposed, standard electrical resistance strain gauges were applied to the top flange of the steel beams and CFRP plates at mid-span. Deflection of the beams at mid-span was also measured using a mechanical dial gauge.

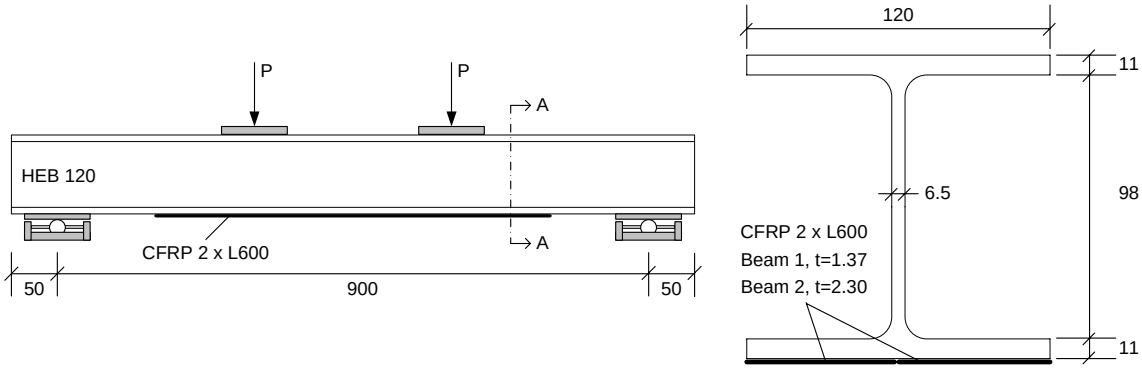

Figure 1. Simply supported test beam subjected to four-point bending, in mm.

The measurement of deformations at the end of the adhesively bonded CFRP plate where strain concentrations were expected was carried out using a 3D digital speckle pattern interferometry (DSPI) system. Speckle interferometric techniques rely on laser light to illuminate a rough surface. The diffusively back-scattered light appears in a noisy and spotted pattern called speckle pattern. Depending on the optical configuration used, this speckle pattern modifies in relation to the local displacement undergone by the surface. The interferometric system detects the optical path difference due to the local displacement and displays it in the form of fringe maps.

Table 1. Properties of steel, adhesive and CFRP plates (linear-elastic range)

Steel	E_s	205000 MPa
	ν	0.3
Adhesive (Sikadur-30®)	E_a	12800 MPa[1.]
	ν	0.25
	$t_{a,\ beam1}$	0.76 mm[2.]
	$t_{a,\ beam2}$	0.60 mm[2.]
CFRP plate (Sika CarboDur S612®)	E_p	174000 MPa[1.]
	ν	0.28
	$t_{p,\ beam1}$	1.37 mm[2.]
	$t_{p,\ beam2}$	2.30 mm[2.]

1. Given by manufacturer
2. Measured values

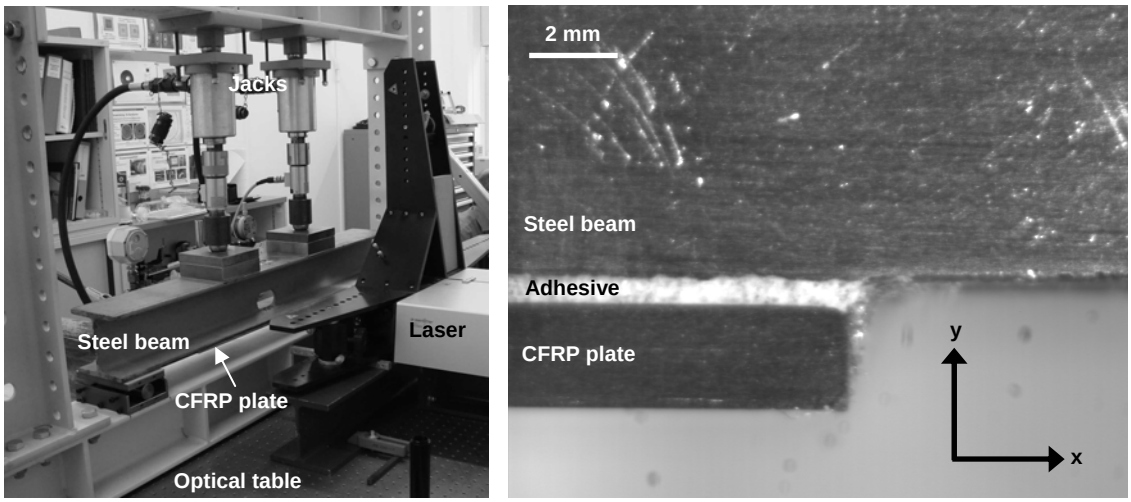

Figure 2. Experimental set-up (left); optical measurement area at plate end, 16x11 mm^2 (right).

Figure 2 (right) shows the measurement area of approximately 16 x 11 mm^2 at plate end. The area was illuminated with a Nd:YVO-laser (wavelength, $\lambda = 532$ nm) sequentially from three directions. At each load level, DSPI phase maps for the three illumination directions were taken with OPTOCAT Software (Breuckmann). A standard four-frame phase-stepping algorithm was applied. The phase maps were transformed to Cartesian displacement components (u, v, w) using the appropriate transformation matrix that was calculated from the geometry of the experimental set-up. This resulted in a sensitivity of 0.299 µm/fringe in-plane (u and v components) and 0.183 µm/fringe out-of-plane (w component). The resulting phase maps after elimination of rigid body in plane translation and in-plane rotation fringes are displayed in Figure 3. The stress transfer through the adhesive layer is clearly seen in the x-displacement field as a rapid change in fringe orientation.

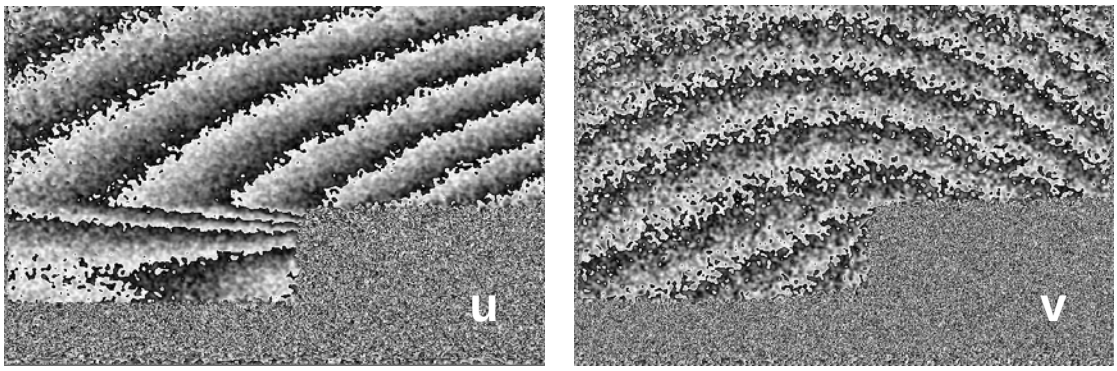

Figure 3. Fringe field for in-plane displacements in x-direction (left) and in y-direction (right). One fringe corresponds to a displacement increment of 0.299 µm.

3 FE MODELING OF PLATE-END STRAINS

A 3D linear-elastic finite element analysis of the strengthened beam was conducted using the commercial finite element code ABAQUS®. The element C3D20R—a three dimensional, 20-node quadratic brick element with a reduced integration scheme and six degrees of freedom at the nodes—was used to model the beam specimen.

In order to model precisely the plate end, a submodelling procedure was carried out. Submodelling is the study of a local part of a model based on an existing solution from a global model. That is, a global solution is obtained using a coarse mesh, interpolated onto the boundary of a locally refined mesh, resulting in a detailed solution in the local area of interest. To avoid

numerical problems, the submodelling was divided into two steps. In the first step, a semi-refined submodel, Submodel 1, was created. Submodel 1 was driven by solutions from the Coarse model. A second, even more refined submodel, Submodel 2, was then created. Submodel 2 was driven by solutions from Submodel 1. Figure 5 shows the coarse and submodels used in the FE analysis. Also shown in Figure 5 are the kinematic boundary conditions required to simulate the planes of symmetry of the quarter-beam model.

The material properties of the adhesive and steel are presented in Table 1 above; for the CFRP the following orthotropic material properties were implemented in the analysis (the orientation of the axes is shown in Figure 4): E_1=9000 MPa, E_2=9000 MPa, E_3=174000 MPa, G_{13}=2000 MPa, G_{23}=4500 MPa, G_{12}=4400 MPa, ν_{13}=0.04, ν_{23}=0.28, ν_{12}=0.28. A convergence study was carried out, whereby further refinement of the element mesh (to the mesh that is shown in Fig. 5, Submodel 2) resulted mainly in an increase in strain at points of singularity, e.g. plate end, steel-adhesive interface. The Submodel 2 mesh presented here includes elements widths of 0.1 mm at the plate end and element heights of 0.06 mm at the plate-adhesive-steel beam interfaces.

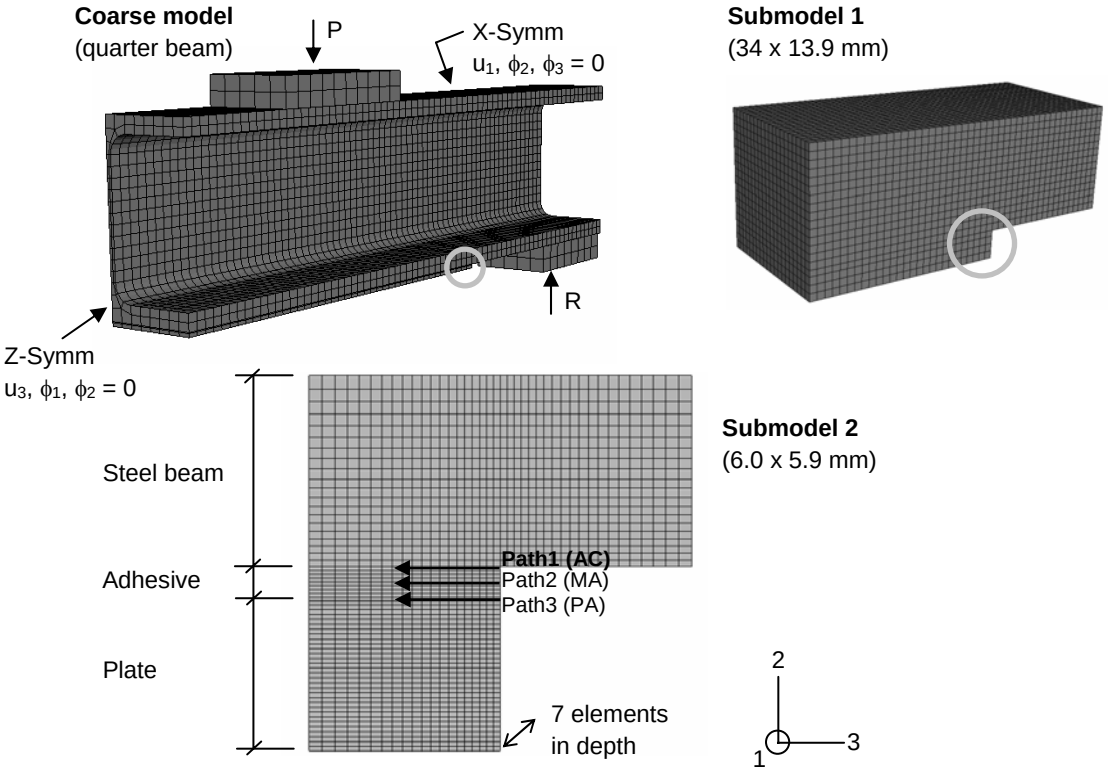

Figure 4. 3D FE model, coarse and submodels (Beam 2).

4 OPTICAL MEASUREMENT AND FEA RESULTS

For quantitative strain analyses and comparison purposes, the optically measured in-plane displacement data were filtered and numerically differentiated. Different fitting strategies were used to average out the noise, including a set of cubic splines within intervals along each line. The polynomial coefficients of the splines were calculated according to a least squares criterion under the boundary condition of continuity of the first and second derivatives of the resulting fit line at the interval borders. The strain values were then calculated numerically from the fit lines. Figure 5 shows the normal and shear strain maps, e22 and e23, in μm/m at plate end, at a load, P, of 40 kN. Only the results from Beam 2 are presented here. On the right in Figure 5 the shear strain clearly reaches a maximum in the adhesive layer near the plate end. For the normal strain,

there seems to be no distinct maximum in the strain field. However it might be drowned in the relatively high noise level or it is highly concentrated. The uncertainty in the strain values from the DSPI evaluation is estimated from the standard deviation over a range of constant strain values. It is found to be approximately 100 μm/m for values obtained from the noisier y-displacement field, and approximately 40 μm/m for values obtained from the x-displacement field.

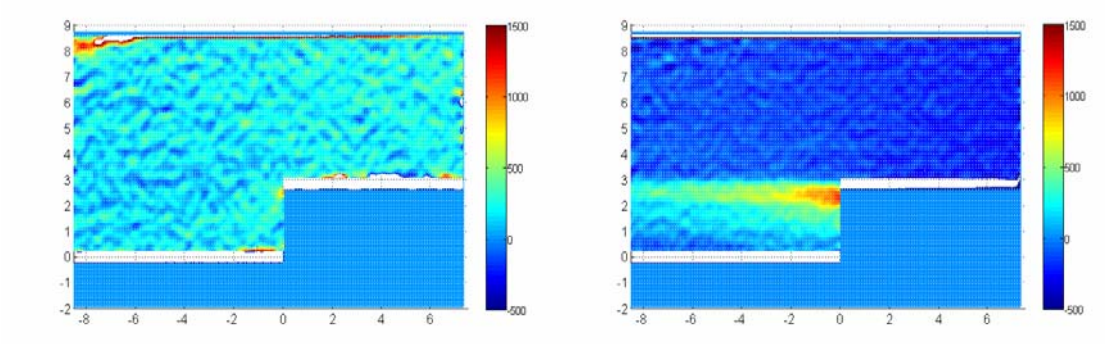

Figure 5. Optical measurement results. Normal (left) and shear (right) strain maps close to plate end, in μm/m.

Figure 6 presents the normal and shear interfacial strains obtained from FE Submodel 2. The results in Figure 6 are shown for a load, P, of 40 kN and are taken along the paths shown in Figure 4. The results are very similar to 2D FEA results presented by Teng et al. (2002). On the left in Figure 6 the normal strains along Paths 1 and 3 diverge at a distance very close to the plate end, whereby the normal strain at the adhesive-steel (AS) interface (Path 1) is considerably higher than the strain at the plate-adhesive (PA) interface (Path 3). This difference has been suggested by others as the reason why debonding failure almost always occurs at the AS interface rather than the PA interface (Rabinovich & Frostig 2000). As expected, the shear strains on the right in Figure 6 tend to zero at plate end; the peak shear strain occurs very close to the plate end (approx. 0.5 mm from the plate end along Path 2), which is due to the thin adhesive layer (0.60 mm). Teng et al. (2002) found in their FEA study that the distance at which the shear peak occurs from the plate end reduces with a reduction in the adhesive layer.

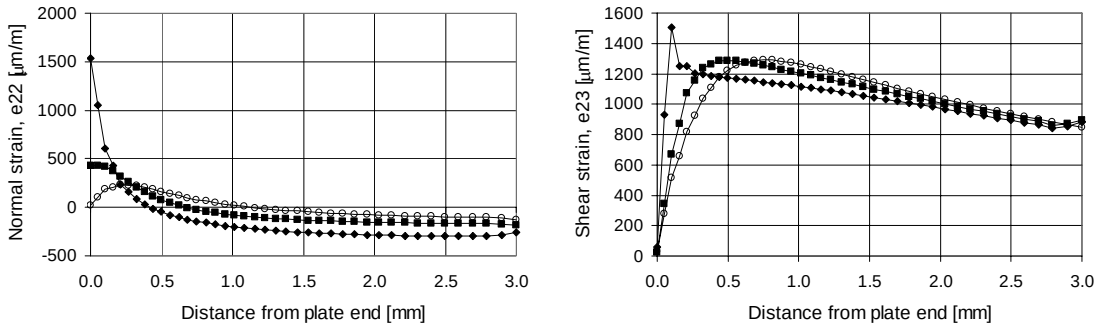

Figure 6. FEA results. a) Normal and b) shear strains close to plate end. —◆— Path 1 (AS), —■— Path 2 (MA), —⊖— Path 3 (PA).

Figure 7 presents the normal and shear strains obtained from Submodel 2 and the shear strains from the optical measurements across the through-thickness of the adhesive (from the plate-adhesive interface to the steel-adhesive interface) and at different distances from the plate end. It is believed that this is the first comparison of numerically obtained plate end strains with measured values ever made. The variation in normal strain across the adhesive confirms the observation from above: the normal strain near plate end is much higher at the AS interface (Path 1) than at the PA interface (Path 3). In Figure 6 (right), a good agreement is seen between

measured and FEA results. A comparison between calculated and measured normal strains could not be made for this round of measurements, due to the high level of noise in the y-direction (as explained above); further tests are planned. The measured results confirm that the shear strain varies strongly across the adhesive layer near the plate end. This variation is less pronounced farther away from the plate end (see e23 curve at 0.439 mm from plate end).

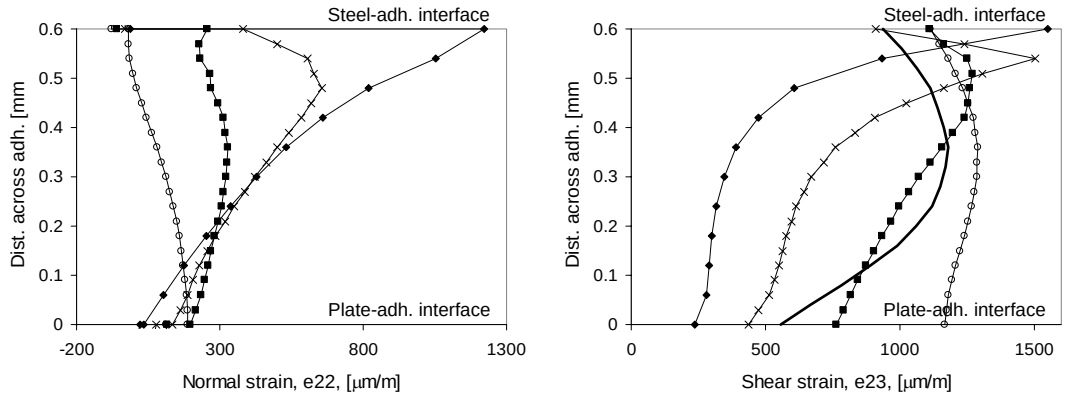

Figure 7. Comparison of FEA and measured results. a) Normal and b) shear strains across adhesive. Distance from plate end: 0.052 mm, 0.104 mm, 0.211 mm, 0.439 mm, approx. 0.1 mm (optically measured).

5 CONCLUDING REMARKS

Small-scale steel beams reinforced with adhesively bonded carbon fiber reinforced polymer (CFRP) plates were subjected to four-point bending. Phase-stepping 3D-digital speckle pattern interferometry (DSPI) was employed to measure the strain concentrations near the end of the CFRP plate, with a special focus on shear and normal strains. Furthermore, a refined finite element analyses (FEA) of the strengthened beam was carried out to predict these strains.

The optical measurement results were able to capture the strain (in particular the shear strain) concentrations that have, up to now, only been shown analytically or using FEA. The magnitude of the measured strains have also compared relatively well to the numerically obtained values. Furthermore, as has been done by a limited number of other authors, the FEA has shown much higher normal strains at the adhesive-steel (AS) interface than at the plate-adhesive (PA) interface, at the CFRP plate end. This difference has been suggested as the reason why debonding failure more commonly occurs at the AS interface rather than the PA interface. It is hoped that this optical measurement technique, in addition to further detailed FEA, will aid in the validation and perhaps refinement of the existing analytical solutions for plate end shear and normal stresses.

6 REFERENCES

Hack, E., and Schumacher, A. 2007. DSPI strain measurement on an externally reinforced bending beam: A comparison of step-by-step addition and pixel shift correlation. *Optics and Lasers in Engineering*, 45(5): 589-595.

Rabinovich, O. and Frostig, Y. 2000. Closed-form higher order analysis of RC beams strengthened with FRP strip. *Journal of Composite Construction*, ASCE, 4: 65-74.

Roberts, TM. 1989. Approximate analysis of shear and normal stress concentrations in the adhesive layer of plated RC beams. *The Structural Engineer*, 67(12): 229-233.

Saadatmanesh, H., and Malek, AM. 1998. Design guidelines for flexural strengthening of RC beams with FRP plates. Journal of Composites for Construction, ASCE, 2(4): 158-164.

Smith, ST., and Teng, JG. 2001. Interfacial stresses in plated beams. *Engineering Structures*, 23: 857-871.

Teng, JG., Zhang, JW., and Smith, ST. 2002. Interfacial stresses in reinforced concrete beams bonded with a soffit plate: a finite element study. *Construction and Building Materials*, 16: 1-14.